Electronic Supplementary Material (ESI) for Journal of Materials Chemistry C.

Crystalline Morphology Formation in Phase-Field Simulations of Binary Mixtures

Supplementary Information

Maxime Siber,[*a,b] Olivier J. J. Ronsin,[a] and Jens Harting [a,b,c]

[a] *Helmholtz Institute Erlangen-Nürnberg for Renewable Energy, Forschungszentrum Jülich, Fürther Straße 248, 90429 Nürnberg, Germany, E-mail: m.siber@fz-juelich.de*
[b] *Department of Chemical and Biological Engineering, Friedrich-Alexander-Universität Erlangen-Nürnberg, Fürther Straße 248, 90429 Nürnberg, Germany*
[c] *Department of Physics, Friedrich-Alexander-Universität Erlangen-Nürnberg, Fürther Straße 248, 90429 Nürnberg, Germany*

Contents

A Composition-Dependence of Kinetic Coefficients

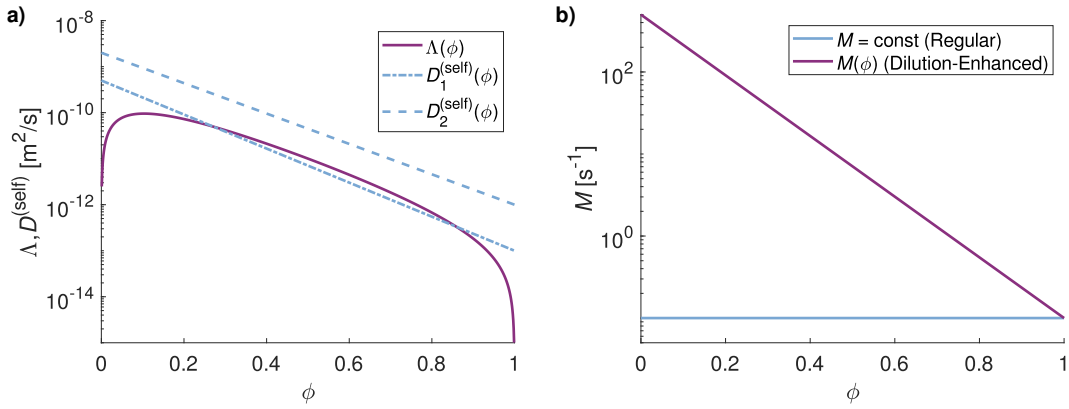

Figure 1: **a)** Composition-dependence of the self-diffusion ($D_1^{(self)}$, $D_2^{(self)}$) and Onsager (Λ) coefficients, as respectively calculated from a logarithmic mean interpolation and the fast mode theory. **b)** Comparison of the evolution of the Allen-Cahn mobility coefficient M with ϕ in the regular and dilution-enhanced crystallization scenarios. In both cases, M_0 = 0.1 s^{-1} was employed.

B Sensitivity of the Liquidus and the Solidus to Thermodynamic Parameter Variations

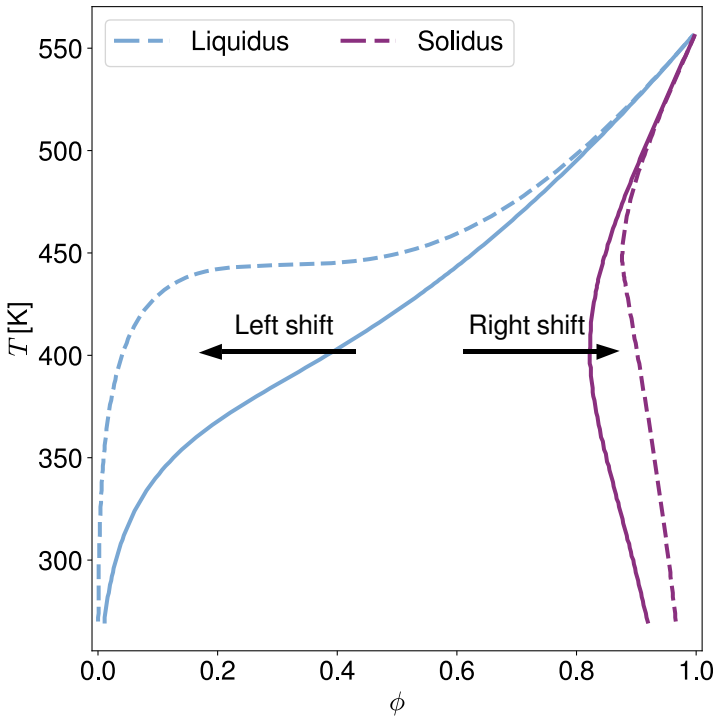

Figure 2: Phase diagram illustrating the shift of the liquidus and solidus curves produced by thermodynamic parameter variations as listed in Tab.1 of the SI. In this particular example, the interaction parameter χ_{aa} is increased from 0.7248 (solid lines) to 1.2648 (dashed lines). All other thermodynamic parameters are identical to those reproduced in Tab.1 of the main article.

Increased Parameter	Effect on liquidus	Effect on solidus
v_0 (with N_1 = const, N_2 = const, ρ = const)	Left shift	Slight left shift
N_1 (when N_2 = 1)	Slight left shift	Slight right shift
N_2 (when N_1 = 1)	Right shift	Right shift
ρ (with N_1 = const)	Left shift	Left shift
ρ (with constant molar mass, i.e N_1 decreasing and N_2 = 1)	Left shift	Left shift
ρ (with constant molar mass, i.e N_2 increasing and N_1 = 1)	Slight left shift	Slight right shift
T_m	Left shift	Left shift
L (with χ_{ca} = const)	Left shift	Left shift
L (with $\chi_{ca} \propto L/RT$)	Left shift	Right shift
W	Negligible	Negligible
χ_{aa}	Left shift	Right shift
χ_{ca}	Right shift	Right shift

Table 1: List of thermodynamic model parameter relevant for the phase diagram computation. Qualitative effects on liquidus and solidus equilibrium curves are specified with respect to an amorphous-crystalline $\phi - T$ phase diagram (see Fig.2) which ϕ-axis represents the volume fraction of the crystalline component ($\phi = 0$ being at the left and $\phi = 1$ at the right limit).

C Formulae for Free Energy Landscape Analysis

This section reports the derivation of the analytical relationships used to locate the energy barrier, the energy minimum, and the pseudo-spinodal in the contour plot of the free energy landscape.
For a given composition ϕ, a minimum or maximum for the total bulk free energy density, defined by

$$G_V^{(bulk)} = \phi\rho\left[q(\psi)W + p(\psi)L\left(\frac{T}{T_m}-1\right)\right] + \frac{RT}{v_0}\left[\frac{\phi\ln(\phi)}{N_1} + \frac{(1-\phi)\ln(1-\phi)}{N_2} + \phi(1-\phi)(\chi_{aa}+\chi_{ca}\psi^2)\right] , \quad (1)$$

is reached when its gradient with respect to the order parameter ψ vanishes, i.e:

$$\frac{\partial G_V^{(bulk)}}{\partial\psi} = \phi\rho\left[q'(\psi)W + p'(\psi)L\left(\frac{T}{T_m}-1\right)\right] + \frac{2RT}{v_0}\phi(1-\phi)\chi_{ca}\psi = 0 . \quad (2)$$

Recalling that $q(\psi)$ and $p(\psi)$ are polynomials in ψ, their derivatives are straightforwardly obtained as $q'(\psi) = 2\psi - 6\psi^2 + 4\psi^3$ and $p'(\psi) = 6\psi - 6\psi^2$. Substituting these into Eq.2 and factorizing with ψ reveals a trivial solution: $\psi_1^* = 0$. In order to find the remaining two, Eq.2 can be simplified to a second order equation in ψ,

$$\left[\rho W + 3\rho L\left(\frac{T}{T_m}-1\right) + \frac{RT}{v_0}(1-\phi)\chi_{ca}\right] - 3\rho\left[W + L\left(\frac{T}{T_m}-1\right)\right]\psi + 2\rho W\psi^2 = 0 , \quad (3)$$

which, once solved, yields

$$\psi_{2,3}^* = \frac{3}{4}\left[1 + \left(\frac{L\left(\frac{T}{T_m}-1\right)}{W}\right)\right] \pm \frac{1}{4}\sqrt{\left(1 - \frac{3L\left(\frac{T}{T_m}-1\right)}{W}\right)^2 - \frac{8RT\chi_{ca}(1-\phi)}{v_0\rho W}} . \quad (4)$$

Respectively, ψ_2^* represents the position of the energy barrier and ψ_3^* the corresponding minimum as a function of ϕ. Considering that $\psi_2^* > 0$ so that the energy barrier is located at positive order parameter values, this formula also provides a lower boundary for the barrier parameter W depending on the heat of fusion L and the crystalline-amorphous interaction parameter χ_{ca} (which is actually dependent on L as well, i.e $\chi_{ca} = C\frac{v_0 N_1 \rho L}{RT}$, with C a proportionality constant):

$$W > 3L\left(1 - \frac{T}{T_m}\right) - \frac{RT}{v_0}(1-\phi)\frac{\chi_{ca}}{\rho} \iff W > L\left[3\left(1-\frac{T}{T_m}\right) - N_1 C(1-\phi)\right] . \quad (5)$$

In a similar manner, the spinodal-like points are attained for a certain ψ when the second derivative of $G_V^{(bulk)}$ (Eq.1) in ϕ equals 0:

$$\frac{\partial^2 G_V^{(bulk)}}{\partial\phi^2} = \frac{RT}{v_0}\left[\frac{1}{N_1\phi} + \frac{1}{N_2(1-\phi)} - 2(\chi_{aa}+\chi_{ca}\psi^2)\right] = 0 . \quad (6)$$

Again, this equation can be expressed as a quadratic form,

$$-2N_1N_2(\chi_{aa}+\chi_{ca}\psi^2)\phi^2 + \left[2N_1N_2(\chi_{aa}+\chi_{ca}\psi^2) - N_1 + N_2\right]\phi - N_2 = 0 , \quad (7)$$

which, upon resolution, gives

$$\phi_{1,2}^* = \frac{1}{2}\left[1 + \frac{1}{2N_1(\chi_{aa}+\chi_{ca}\psi^2)} - \frac{1}{2N_2(\chi_{aa}+\chi_{ca}\psi^2)} \pm\sqrt{\left(1 + \frac{N_2-N_1}{2N_1N_2(\chi_{aa}+\chi_{ca}\psi^2)}\right)^2 - \frac{2}{N_1(\chi_{aa}+\chi_{ca}\psi^2)}}\right] . \quad (8)$$

In addition, the pseudo-binodal points can then be obtained for each ψ with a numeric routine, as for instance the one described by Horst [1][2].

D Sensitivity Study: Additional Parameter Variations

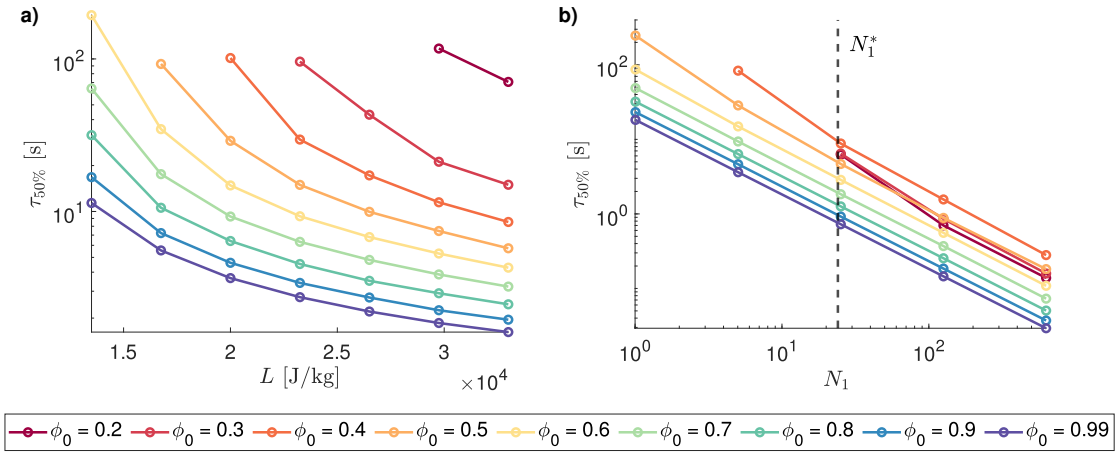

Figure 3: **a)** Sensitivity of the crystallization kinetics to variations of L (with $\chi_{ca} = 0.1648\frac{v_0 N_1 \rho L}{RT}$). **b)** Sensitivity of the crystallization kinetics to variations of N_1. The critical value $N_1^* \simeq 24.031$, beyond which an initial amorphous-amorphous demixing accelerates crystallization for the lowest blend ratios, is calculated by solving the equation describing the threshold criterion for AAPS (Eq.17 in the main article) for N_1 with χ_{aa} = 0.7248. All other simulation parameters are identical to those reproduced in Tab.1 of the main article.

E Diffusion-Limited Crystallization: Transformation Kinetics

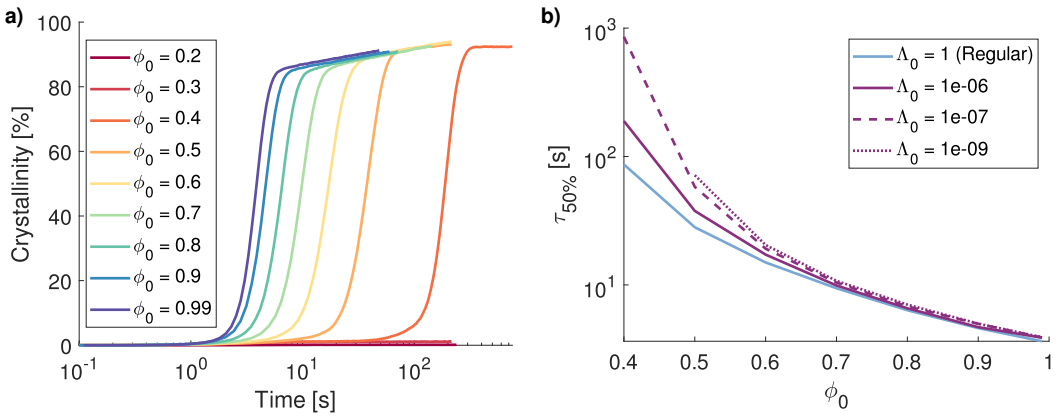

Figure 4: **a)** Transformation kinetics at different blend ratios for a diffusion-limited system. Except for Λ_0 = 10^{-6}, all simulation parameters are identical to those reproduced in Tab.1 of the main article. **b)** Comparison of the crystallization half-time as a function of blend composition in the diffusion-limited and regular crystallization regimes.

F Demixing-Assisted Crystallization: Transformation Kinetics

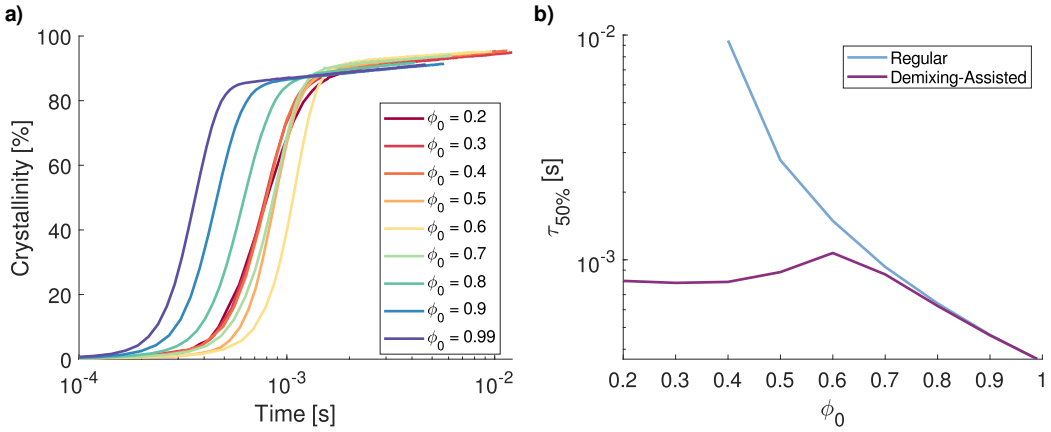

Figure 5: **a)** Transformation kinetics at different blend ratios for an immiscible binary mixture. Except for χ_{aa} = 1.2648 and M_0 = 1000 s^{-1}, all simulation parameters are identical to those reproduced in Tab.1 of the main article. **b)** Comparison of the crystallization half-time as a function of blend composition in the demixing-assisted and regular crystallization regimes (with M_0 = 1000 s^{-1}).

G Demixing-Assisted Crystallization: Additional Morphology Formation Pathways

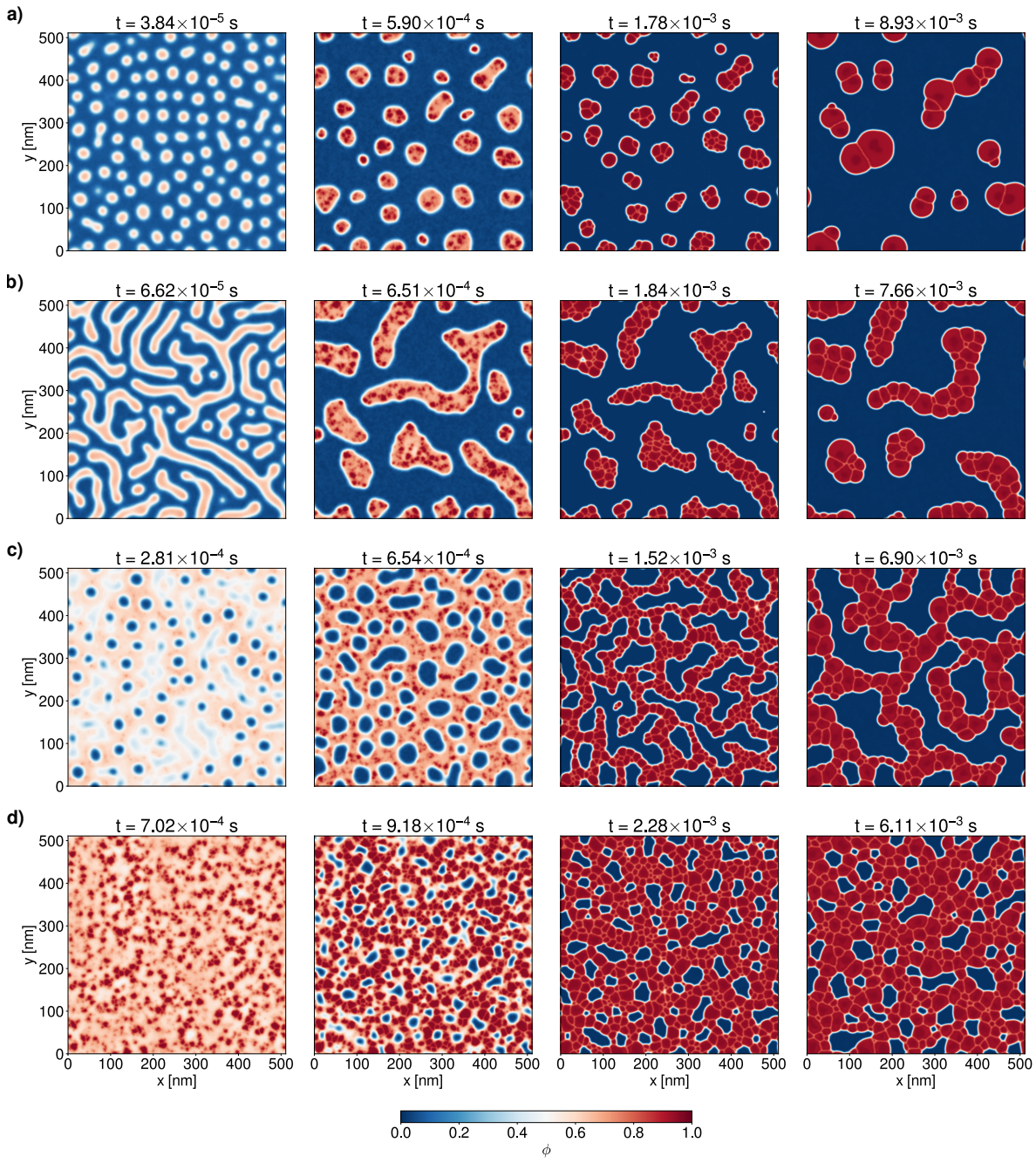

Figure 6: Progress of crystallization simulated for the immiscible system (represented by the phase diagram Fig.8-a in the main article) at T = 333 K and blend ratios **a)** ϕ_0 = 0.2, **b)** ϕ_0 = 0.3, **c)** ϕ_0 = 0.5, and **d)** ϕ_0 = 0.7. For all simulations, the parameters are identical to Tab.1 of the main article, except M_0 = 1000 s^{-1} and χ_{aa} = 1.2648. In the cases **a)**, **b)** and **c)**, crystals start to nucleate and grow during the coarsening stage of the initial spinodal decomposition. The crystallization is triggered in the domains where the solute is in majority and grain boundary coarsening also takes place once crystals impinge. For comparison, configuration **d)** presents the crystallization process for a blend ratio outside of the binodal interval. Here, crystal nucleation and growth occurs directly and solute in the initially mixed amorphous phase is homogeneously consumed without spinodal decomposition or local formation of solvent-rich droplets by NG.

H Dilution-Enhanced Crystallization: Morphology Formation Pathways

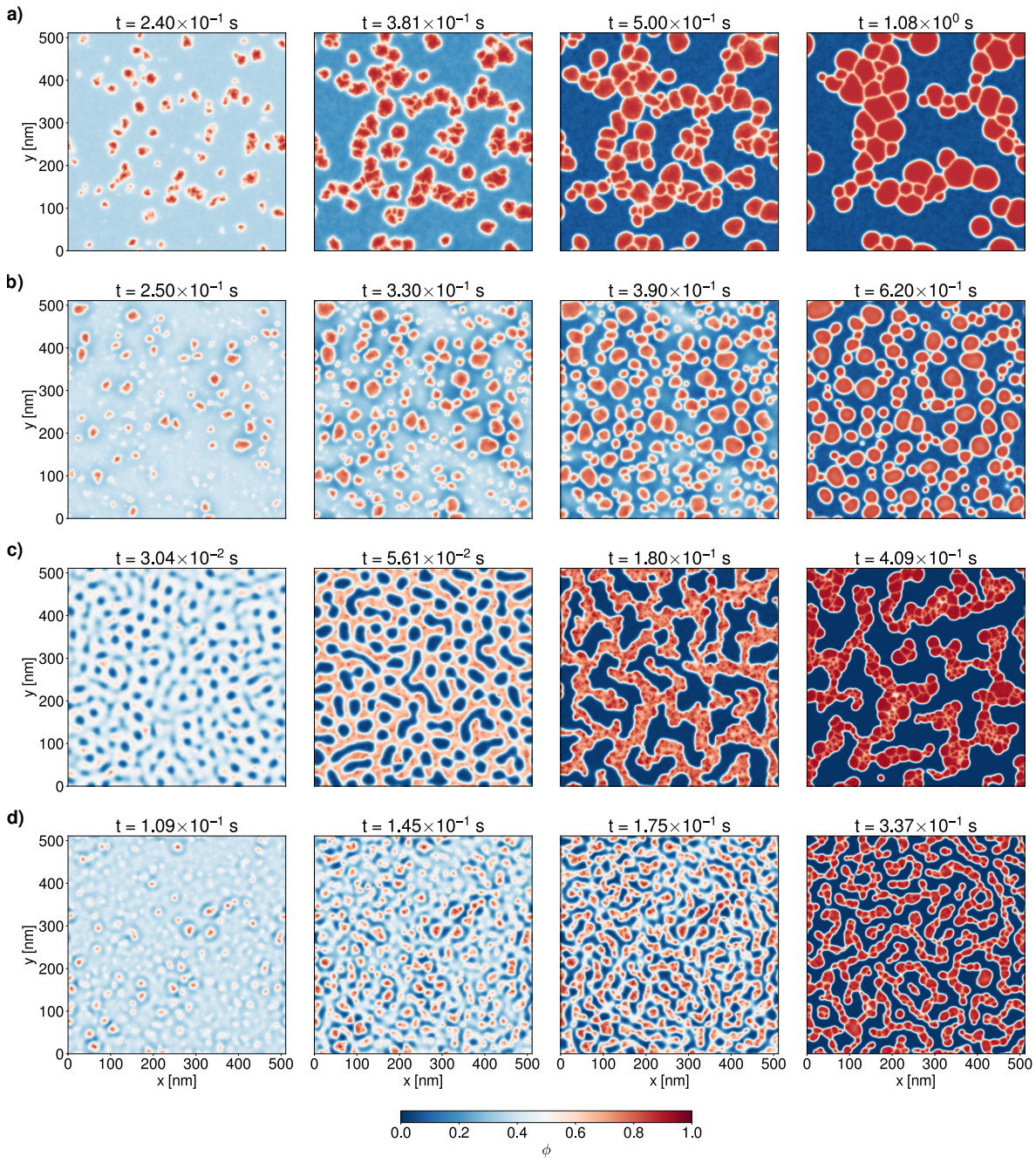

Figure 7: Progress of crystallization for a binary blend in the dilution-enhanced regime (i.e. $M(\phi)$) at T = 333 K and blend ratio ϕ_0 = 0.4 with **a)** regular, **b)** diffusion-limited (Λ_0 = 10^{-4}), **c)** demixing-assisted (χ_{aa} = 1.2648, Λ_0 = 10^{-3}), and **d)** combined immiscible and diffusion-limited behavior (χ_{aa} = 1.2648, Λ_0 = 10^{-4}). Besides the specified modifications, all simulation parameters are identical to those reproduced in Tab.1 of the main article.

References

1. Horst, R. Calculation of Phase Diagrams Not Requiring the Derivatives of the Gibbs Energy Demonstrated for a Mixture of Two Homopolymers with the Corresponding Copolymer. *Macromolecular Theory and Simulations* **4,** 449–458 (1995).
2. Horst, R. Calculation of Phase Diagrams Not Requiring the Derivatives of the Gibbs Energy for Multinary Mixtures. *Macromolecular Theory and Simulations* **5,** 789–800 (1996).